New Insights into the Behavior of Bovine Serum Albumin Adsorbed onto Carbon Nanotubes: Comprehensive Spectroscopic Studies

ARTICLE *in* THE JOURNAL OF PHYSICAL CHEMISTRY B · APRIL 2010

Impact Factor: 3.3 · DOI: 10.1021/jp100903x · Source: PubMed

New Insights into the Behavior of Bovine Serum Albumin Adsorbed onto Carbon Nanotubes: Comprehensive Spectroscopic Studies

Xingchen Zhao, Rutao Liu,* Zhenxing Chi, Yue Teng, and Pengfei Qin

School of Environmental Science and Engineering, Shandong University, 27 Shanda South Road, Jinan 250100, P.R. China

Received: January 30, 2010; Revised Manuscript Received: March 18, 2010

Bovine serum albumin (BSA) nonspecifically binds to well-dispersed multiwalled carbon nanotubes (MWCNTs), forming a stable bioconjugate. After accounting for the inner filter effect, we found the fluorescence intensity of BSA was quenched by MWCNTs in static mode, which was authenticated by lifetime measurements and Stern−Volmer calculations. The thermodynamic parameters $\Delta G°$, $\Delta S°$, and $\Delta H°$ were $-9.67 \times 10^3 + 2.48 \times 10^3 \ln \lambda$ J·mol^{-1}, $41.0 - 0.828 \ln \lambda$ J·mol^{-1}·K^{-1}, and $7.30 \times 10^3 + 2.23 \times 10^3 \ln \lambda$ J·mol^{-1} ($\lambda < 1 \times 10^{-4}$), respectively, which shows a spontaneous and electrostatic interaction. Scatchard analysis and UV−visible results provide statistical data concerning changes in the microenvironment of amide moieties in response to different doses of MWCNTs, revealing different behavior of the BSA molecules. The absorption spectra also show that the tertiary structure of the protein was partially destroyed. The content of secondary structure elements of BSA was changed by the tubes. This work elucidates the interaction mechanism of BSA and MWCNTs from a spectroscopic angle.

1. Introduction

Carbon nanotubes (CNTs) have fascinated human beings since their discovery by Iijima because of their fine electronic, optical, thermal, and mechanical properties.[1] Thus, wide application of CNTs is on the way and professional and public exposure to nanomaterials is predicted to increase dramatically in the coming years.[2]

However, uncertainty over the potential hazardous effects of CNTs on human health and the environment has become of great concern, as illustrated by the editorials on the bioeffects, environmental and physical influences of nanoscaled particles published in *Science* and *Nature*.[3,4] Thus, there is an imperative demand to determine how toxic CNTs actually are.

Previous studies have shown toxicity for nanotubes. Early animal toxicology studies showed that pulmonary deposition of single-walled carbon nanotubes (SWCNTs) resulted in acute pulmonary inflammation as well as chronic responses.[5] Wang injected well-dispersed CNTs with hydroxyl groups into mice and demonstrated that the CNTs can move freely in compartments and tissues and finally accumulate in the liver and kidney.[6] As for the influence targeted to proteins, however, the information is very limited. Azamian et al. found that ferritin attached firmly onto the surface of SWCNTs which increased the solubility of SWCNTs dramatically.[7] Matsuura et al. discovered the conjugation of BSA onto SWCNTs. The three-dimensional structure of BSA changed followed by the exposure of hydrophobic groups.[8]

Clearly, detailing protein structural changes caused by CNTs would be most valuable. Spectroscopic study holds promise as a way of coping with the puzzle. In this work, we used fluorescence spectroscopy and calculated the constants and thermodynamic parameters of the interaction to determine how BSA and MWCNTs interact. For further study, ultraviolet−visible absorption spectroscopy and CD were applied, demonstrating MWCNTs did damage the secondary and tertiary structure of the protein, which was different from the report by Huang.[9] This paper not only provides the detailed behavior of BSA molecules but also creates a framework for analyzing the biocompatibility of nanoparticles in terms of the biological behavior of biomacromolecules.

2. Experimental Section

2.1. Reagents. MWCNTs were purchased from Shenzhen Nanotech Port Co., Ltd. (Shenzhen, China). All MWCNTs were synthesized by chemical vapor deposition. The purity was higher than 95%, and the catalyst residue was less than 0.2%. NaH_2PO_4, Na_2HPO_4, HNO_3, H_2SO_4, and NaOH were all purchased from Tianjin Tianda Chemical Reagent Co., Ltd. (Tianjin, China). Phenylbutazone, flufenamic acid, and digitoxin were produced by Tokyo Chemical Industry Co., Ltd. (Tokyo, Japan). Bovine serum albumin (BSA) was bought from Sinopharm Chemical Reagent Beijing Co., Ltd. (Beijing, China), and was dissolved in ultrapure water to form a 0.5 g/L solution, and then preserved at 4 °C for later use. All solutions were prepared with ultrapure water.

2.2. Apparatus. In all the work, 220 nm pore filter membranes (Shanghai Mili Co., Ltd.), a pHs-3C pH meter (Shanghai Pengshun Scientific Instrument Co., Ltd.), KQ-100E ultrasonic cleaner (Jiangsu Kunshan Ultrasonic Instrument Co., Ltd.), and electric blender (Jintan Xiaoyang Electronic Instrument Factory) were used for sample preparation. FTIR-8400S Fourier transform infrared spectroscopy (Shimadzu, Japan) and Q600SDT thermogravimetric analyzer (TA Instruments, U.S.) were used for characterization of CNTs. The ultraviolet−visible absorbance spectra (UV−vis) were recorded on a UV-2450 spectrometer (Shimadzu, Japan) in a 1 cm quartz cell. Transmission electron microscopy (TEM) images were captured using a JEM-2100 transmission electron microscope (JEM Ltd. Tokyo, Japan) operated at 80 kV. Steady-state fluorescence spectra were measured using a FL-4500 fluorescence spectrophotometer (Hitachi Co. Ltd., Tokyo, Japan). Circular dichroism (CD)

* To whom correspondence should be addressed. Phone/Fax: 86-531-88364868. E-mail: rutaoliu@sdu.edu.cn.

10.1021/jp100903x
Published on Web 04/07/2010

spectra were taken by a J-810 spectropolarimeter (Jasco, Japan) under constant nitrogen flush.

2.3. Preparation of Soluble MWCNTs. ***2.3.1. Purification of MWCNTs.*** To purify the commercial MWCNTs, a pristine sample of nanotubes (5 g) was first immersed in 0.5 L of 2 M nitric acid and stirred for 36 h. Upon cooling, the solution was transferred to polytetrafluoroethylene centrifuge tubes and spun at 2400*g* for 10 min. The supernatant acid was decanted off, replaced by deionized water, and vigorously shaken to resuspend the solids, followed by a second centrifuge−decant cycle. The solids were then washed twice with 1 L of ultrapure water.

2.3.2. Functionalizing MWCNTs with Carboxyl Groups. To make the nanotubes soluble in water, we functionalized them with carboxyl groups as follows. One gram of the purified MWCNTs was suspended in 600 mL of a 3:1 mixture of concentrated H_2SO_4/HNO_3 and was subjected to ultrasonic treatment for 25 h at 60 °C. The resultant suspension was poured in 400 mL of water afterward, and the larger cut MWCNTs were collected on a 220 nm pore filter membrane and rinsed with 20 mM NaOH solution. Finally, they were dried in a vacuum to obtain soluble powder and were characterized by FTIR and TGA (thermogravimetric analyzer).

2.3.3. Accurate Calibration of MWCNT Solution. In order to avoid bundling and obtain a well-dispersed MWCNT solution, we measured different concentrations of MWCNT solutions on a UV−vis spectrometer at 907 nm where the absorbance of MWCNTs was not too high. Then, a working curve illustrating the UV−vis absorption spectra of these samples was plotted with the dependence of absorbance on the solution concentration obeying the Lambert−Beer law (SI Figure 1, Supporting Information). MWCNT solution of a certain concentration was centrifuged, and the supernatant was obtained. The absorbance was measured, and the final concentration of the supernatant, which was used as the stock solution, was determined from the calibration curve.

2.4. Methods. For the fluorescence measurement, MWCNT solution was added into the protein solutions in sequence. Both MWCNT concentration and BSA concentration were calculated by weight for consistency. The systems were excited at 278 nm, and the emission wavelength was adjusted from 290 to 410 nm with a scanning speed of 1200 nm/min. Excitation and emission slit widths were both set to 5.0 nm. The scanning voltage was set to 750 V. The binding site was characterized by a fluorescence experiment using three molecular probes (digitoxin, phenylbutazone, and flufenamic acid) with fixed concentrations of BSA and MWCNTs.

Time-resolved fluorescence measurements were carried out using a FLS920 Combined Fluorescence Lifetime and Steady State Spectrometer (Edinburgh, U.K.). BSA was fixed at a concentration of 10 mg/L and was excited at 278 nm.

CD measurements were operated over the range 190−240 nm at a scan rate of 200 nm/min. The spectra were measured in a temperature-controlled 1 cm path length cell, and each spectrum was the average of two scans.

For UV−vis absorption spectra, a series of MWCNT solutions with different concentrations and 150 mg/L BSA solutions were added to eight 10 mL volumetric flasks in sequence, and then diluted with ultrapure water to the mark. The equilibrated solution was poured into quartz cells and scanned in the ultraviolet range of 190−350 nm using MWCNT solutions as references.

MWCNT powder was grounded with highly purified KBr crystal in an agate mortar and the mixture was pressed to form a pellet. The FTIR spectra were measured by a FTIR-8400S spectrometer with a resolution of 1 cm^{-1}.

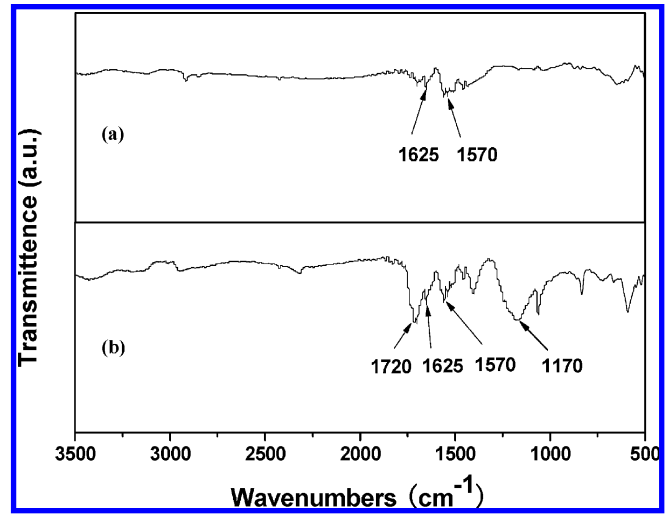

Figure 1. FTIR spectra for MWCNTs: (a) unmodified MWCNTs; (b) carboxylated MWCNTs.

We use phosphate buffered saline (PBS) as buffer throughout. All measurements were performed at room temperature (25 °C) unless otherwise indicated.

3. Results and Discussion

3.1. Characterization of Functionalized MWCNTs. MWCNTs functionalized through carboxylation were characterized by FTIR and TGA. In Figure 1, the peak at 1570 cm^{-1} is assigned to the C═C stretching mode associated with MWCNTs sidewall defects. The weak peak at 1625 cm^{-1} seen in the two spectra shown in this figure is associated with traces of water in the KBr used for making the pellet. The peak at 1720 cm^{-1} in Figure 1b clearly represents the C═O stretching mode in the H_2SO_4/HNO_3 treated MWCNTs, and the strong absorption peak at about 1170 cm^{-1} is typical for the stretching of C−O. The data indicates successful addition of COOH groups onto the uncapped ends of the graphene walls and to the edges of the holes. During thermal gravimetric analysis (TGA) in air (SI Figure 2, Supporting Information), the rate of weight change decreases initially because of the adsorbed water at about 45 °C. Then, there is another weight change at 200−400 °C, indicating the decomposition of COOH. Compared with the carboxylated nanotubes, unmodified MWCNTs are more stable with a decomposition temperature of 560 °C or so.

3.2. Conformation Investigation and Mechanism. ***3.2.1. The Influence of MWCNT Dose on the Fluorescence Intensity of BSA.*** In order to examine the interaction of MWCNTs with BSA, the fluorescence spectra were measured in PBS of pH 7.4 and representative spectra are presented in Figure 2A. A gradual increase of the MWCNT concentration in the solutions of BSA resulted in a decrease of fluorescence intensity and a slight blue shift at the emission maxima.

Mu and co-workers[10] employed fluorescence spectra of the BSA−MWCNT system to investigate the conformational changes of BSA. They gave the direct measuring results without considering the inner filter effect (IFE) which could interfere with the results. BSA is able to increase the solubility of CNTs to a large extent.[7,8,11−13] However, at increasing concentrations of a fluorescent substrate and quencher, the increasing absorbance of excitation and/or emission radiation introduces IFE that decreases the fluorescence intensity and results in a nonlinear relationship between the observed fluorescence in-

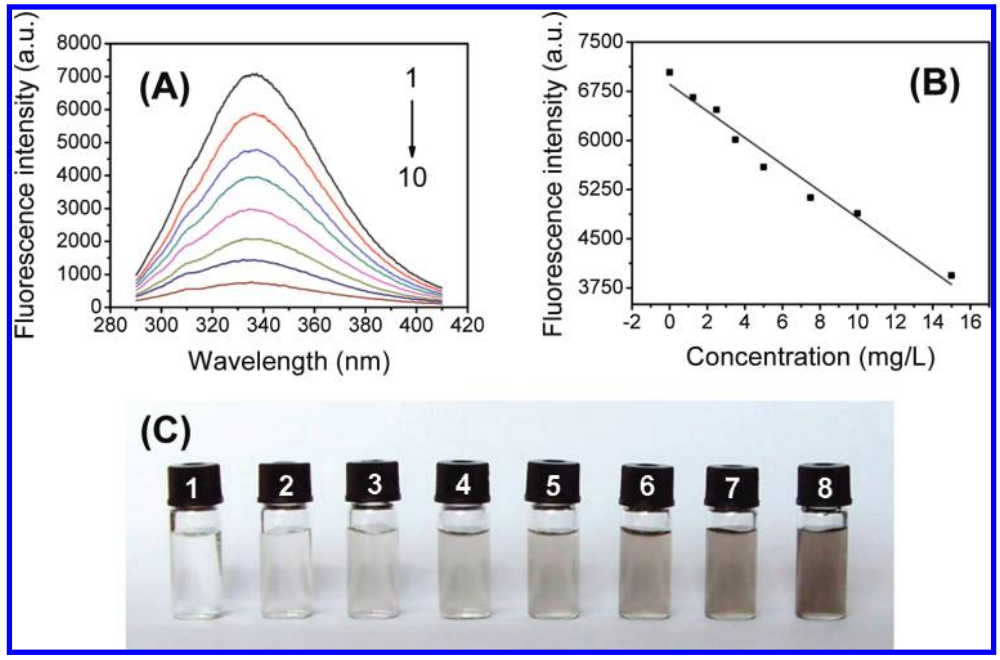

Figure 2. (A) Fluorescence quenching of BSA (50 mg/L) observed by increasing MWCNT concentration. The final concentrations of MWCNTs from top to bottom are 0, 1.25, 2.5, 3.5, 5, 7.5, 10, and 15 mg/L. (B) Plot of fluorescence quenching for BSA at 335 nm after correction of IFE for part A. (C) Photograph of the solutions corresponding with part A.

tensity and the concentration of the fluorophore.[14] Typically, IFE consists of two aspects: primary inner filter effect (pIFE) refers to the absorption of excitation radiation, and secondary inner filter effect (sIFE) refers to the absorption of emission radiation. According to Gu,[15] the fluorescence of a mixture showing IFE can be calculated when absorbance effects are corrected by multiplying appropriate correction factors, as shown in eq 1:

$$F_{ideal}(\lambda_{ex},\lambda_{em}) = F_{obs}(\lambda_{ex},\lambda_{em})CF_p(\lambda_{ex})CF_s(\lambda_{em}) \approx F_{obs}(\lambda_{ex},\lambda_{em})10^{(A_{em}+A_{ex})/2} \quad (1)$$

where CF_p is the correction factor for pIFE, which depends on the total absorbance of the sample at λ_{ex}, whereas CF_s is the correction factor for sIFE, which depends on the total absorbance of the sample at λ_{em}. A_{ex} and A_{em} represent the absorbance at the fluorescence excitation and emission wavelengths, respectively. F_{obs} is the observed fluorescence. By exploiting eq 1, we obtained a plot (Figure 2B) of fluorescence quenching with the increasing concentration of MWCNTs corrected for IFE.

As the most plentiful protein in plasma and the most important carrier in blood, BSA contains three intrinsic fluorophores: tryptophan, tyrosine, and phenylalanine. Of all three intrinsic fluorophores, tryptophan moieties contribute most to the fluorescence intensity. The BSA molecule has two tryptophan residues that possess intrinsic fluorescence: Trp-212 is located within a hydrophobic binding pocket of the protein, and Trp-134, on the surface of the albumin molecule.[16] A valuable feature of intrinsic fluorescence of proteins is the high sensitivity of tryptophan to its microenvironment. Commonly, emission spectra change in response to protein conformational transitions, or denaturation. According to the principle of micelle sensitization in spectrophotometric determinations, the fluorescence intensity of tryptophan buried inside of BSA is much stronger than that in aqueous solution at the same concentration.[17]

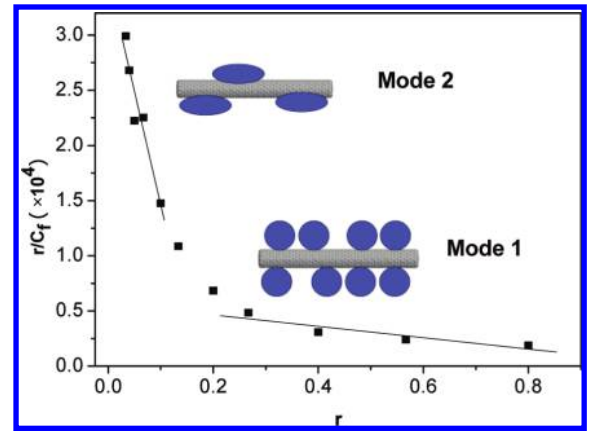

Figure 3. Scatchard plot showing two modes of BSA molecule binding to MWCNTs: mode 1, high ratio of BSA/MWCNTs; mode 2, low ratio of BSA/MWCNTs when λ is 10^{-6}.

The fluorescence intensity of BSA becomes weak after 20 min of thermal denaturation at 90 °C, resulting from disintegration of BSA structure and entire exposure of tryptophan residues to the solvent.[17] Similarly, the fluorescence quenching of the system demonstrated that with the increasing concentration of MWCNTs the tryptophans in the hydrophobic fold were gradually exposed to the aqueous milieu. In addition to this, the blue shift in the position of the emission maximum corresponds to changes of the polarity around the chromophore molecule, which is in accordance with the quenching.

We did saturation binding experiments to explore the binding mode. By fixing the concentration of BSA, the fluorescence intensity of the mixture was measured with MWCNT concentration from a very low level to a rather high one. A nonlinear Scatchard curve at 298 K was plotted (Figure 3). As the molecular weight is not definite, the molar concentration of MWCNTs cannot be accurately determined, so in this work we used weight concentration multiplied by λ as a pseudo molar concentration. For one of the nanotubes we used here, the number of carbon molecules in it would not be less than 1000,

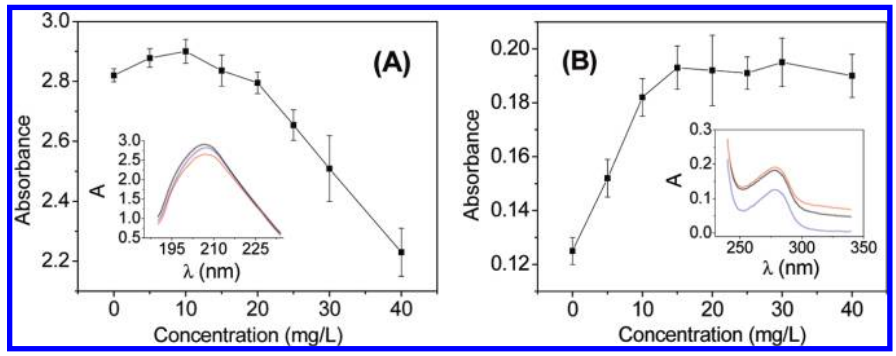

Figure 4. Absorbance of BSA at 208 nm (A) and 278 nm (B) in the presence of MWCNTs. MWCNTs and buffer were subtracted. The concentration of BSA was fixed at 150 mg/L. Shown in the inset are the corresponding absorption spectra with different concentrations of MWCNTs. Blue, black, and red curves stand for 0, 10, and 25 mg/L MWCNTs, respectively. Error bars are the standard deviations of three measurements.

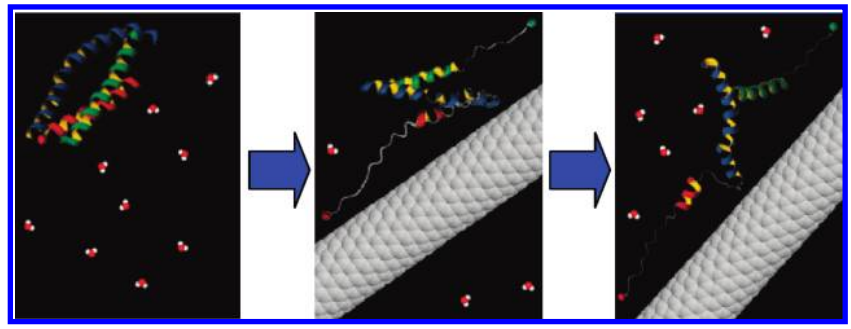

Figure 5. Schematic procedure for the microenvironment changes of amide moieties, taking an α-helix as an example.

so λ should be no more than 1×10^{-4}. The nonlinearity of the Scatchard plot illustrates that the MWCNTs are bound to multiple binding sites of BSA. At a high ratio of BSA/MWCNTs, K_A (equilibrium binding constant) and n (numbers of binding sites) were $0.0515/\lambda$ M^{-1} and 1.1, which shows that most of the MWCNTs were coated thickly by protein molecules with weak adhesive strength. Nevertheless, at a lower BSA/MWCNT ratio, K_A and n became $2.05/\lambda$ M^{-1} and 0.171, indicating that BSA bound more firmly to MWCNTs with more protein binding sites occupied.

3.2.2. UV−vis Investigation on the Conformational Changes of BSA. UV−vis absorption measurement is a simple but efficacious method to explore structural changes and show complex formation. As shown in Figure 4A, there is a strong absorption band at around 208 nm which is mainly due to the transition of $\pi \rightarrow \pi^*$ of BSA's characteristic polypeptide backbone structure C═O.[18,19] Besides this, the absorption peak at about 278 nm can provide us with information about the three buried aromatic amino acids: Trp, Tyr, and Phe.[20]

When MWCNTs were gradually added, the absorbance at 208 nm first increased slightly and then decreased dramatically, indicating disturbances to the microenvironment around the amide bonds in the protein. This strange phenomenon is likely to be associated with the effect of the polar solvent, water, and disturbances by the conjugated π electronic cloud on the surface of the MWCNTs. Compared with the π electron cloud which exists in the ground state, the π^* electron cloud has higher polarity because of the formation of an antibonding orbital between C and O in the excited state. Thus, as a polar solvent, water has a stronger ability to lower the energy of a π^* electron cloud rather than a π electron cloud, although it lowers the energy levels of both states. In this case, when the energy required is low, the $\pi \rightarrow \pi^*$ transition undergoes a bathochromic shift and a hypochromic effect is observed.[21−24]

It is thus easier to comprehend the interesting process displayed in the UV−vis spectra. In a water milieu, amide moieties which are exposed to a water environment experience a low-energy $\pi \rightarrow \pi^*$ transition when absorbing ultraviolet radiation. However, the small amount of nanotubes added into the protein solution supplanted the H_2O, creating a nonpolar environment for the amide moieties, leading to a higher energy gap of the transition, which caused a hypsochromic shift and the hyperchromic effect seen in the spectra. With the increasing amount of nanotubes, fewer BSA molecules attached to a single tube. The BSA molecules further denatured and the main chain uncurled, resulting in a greater possibility to encounter H_2O, especially for the amide moieties that used to be in the hydrophobic pocket of the protein. An α-helix is taken as an example in Figure 5. Normally, water molecules can only touch amide moieties on the surface of the BSA molecule because the others are in the hydrophobic pocket. When a small amount of MWCNTs is added, fewer water molecules can approach the amide moieties now blocked by the nanotubes. However, eventually, the loosened structure may let more water molecules in, as the protein binds to the MWCNTs and unfolds.

Meanwhile, the absorption peaks at approximately 278 nm increased by degrees and finally stabilized (Figure 4B), which shows that more aromatic acid residues were extended into the aqueous environment. Trp-212, which was originally buried in a hydrophobic pocket, was exposed to an aqueous milieu to a certain degree. This result indicated that the microenvironment of the three aromatic acid residues was altered and the tertiary structure of BSA was destroyed.

3.2.3. The Influence of MWCNTs on BSA Structure Evaluated by CD Spectroscopy. CD spectroscopy, a sensitive technique, is commonly used to study secondary protein conformations in solution. To gain a better understanding of the conformational behavior of BSA in the presence of MWCNTs, CD spectroscopy was performed on different BSA−MWCNT mixtures. It can be seen in Figure 6 that the CD spectra of BSA at pH 7.4 exhibited two negative double humped peaks in the ultraviolet region at 208 and 222 nm, which

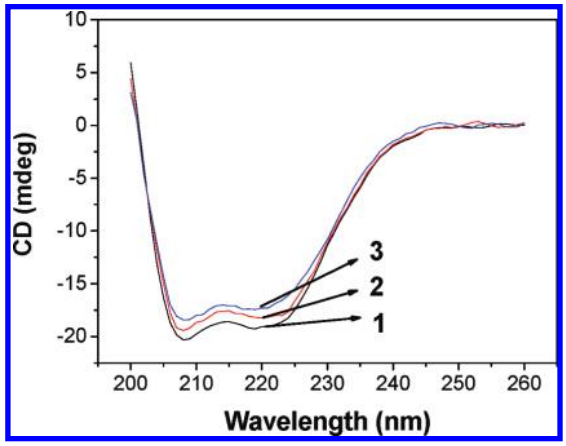

Figure 6. CD spectra of BSA in the absence or presence of MWCNTs. The BSA concentration was 10 mg/L in 20 mM PBS buffer solution (pH 7.4). The final concentrations of MWCNTs were 0, 2, and 5 mg/L from 1 to 3.

TABLE 1: Secondary Structure of BSA with Different Concentrations of MWCNTs in Accordance with Figure 5

	content (%)			
sample	α-helix (±2%)	β-sheet (±1%)	β-turn (±1%)	random coil (±2%)
1	59.3	7.5	8.2	25.3
2	52.6	15.5	7.8	24.1
3	45.1	24.9	6.8	23.5

is characteristic of an α-helical structure of the protein. The fractions of α-helix, β-sheet, β-turn, and random coil are shown in Table 1. It is apparent that, compared with the native protein, the α-helix structure content is decreased, giving evidence that MWCNTs bind to the amino acid residues of the main polypeptide chain of BSA and destroy the hydrogen bonding networks.[25]

3.2.4. Effect of Ionic Strength. The fluorescence intensity of the protein was significantly affected by ionic strength (NaCl concentration in this study) in protein and MWCNT mixed solution. It is known that electrostatic interactions play a key role in the interaction between NaCl and proteins.[26] In SI Figure 3 (Supporting Information), the ionic strength initially gives rise to an increase in the fluorescence intensity and finally has no evident influence on the intensity, indicating the fluorophores were again buried in a hydrophobic environment; that is, ionic strength has an antagonistic effect on the binding of BSA and MWCNTs and electrostatic interactions indeed influence the binding.

3.2.5. TEM Characterization of the BSA−MWCNT System. TEM images were taken to confirm the integrity of MWCNTs after the harsh oxidation reaction and to observe the combination of BSA and MWCNTs. Figure 7A shows the pristine MWCNTs twining around each other and attached to amorphous carbon and other impurities. It is clear that, after purification and chemical transformation on the surface, the nanotubes became neater, tidier, and shorter. In addition to this, they were more scattered and intertwining tubes are rarely observed, indicating good dispersion. BSA was dissolved uniformly in water originally; however, after mixing with MWCNTs, the protein adsorbed and aggregated onto the surface of the tubes.

3.3. Thermodynamic Study of the Protein−Nanotube Interaction. ***3.3.1. Determination of the Quenching Mechanism.*** In order to further investigate the quenching form of BSA, the well-known Stern−Volmer equation (eq 2) was used to analyze the quenching data.

$$F_0/F = 1 + K_q\tau_0[Q] = 1 + K_{SV}[Q] \quad (2)$$

where F_0 and F represent the fluorescence intensities in the absence and in the presence of quencher, K_q is the quenching rate constant of the biomolecule, K_{SV} is the dynamic quenching constant, τ_0 is the average lifetime of the molecule without quencher, 10^{-8}, and [Q] is the concentration of the quencher.[17]

F_0/F versus [Q] was plotted at 283, 298, and 313 K (Figure 8). K_{SV}, calculated by linear regression of the plots, are 0.0326, 0.0512, and 0.0686/λ L·M^{-1}, respectively, rising with temperature. Thus, we preliminarily drew the conclusion that this quenching process is dynamic quenching; that is, quenching was probably initiated by intermolecular collisions. Since the fluorescence lifetime of the biopolymer was 10^{-8} s,[17] the quenching rate constant K_q could be calculated according to the equation $K_q = K_{SV}/\tau_0$. For BSA, τ_0 is known to be approximately 10^{-8} s;[27] thus, $K_q = 3.26 \times 10^9$, 5.12×10^9, and $6.86 \times 10^9/\lambda$ L·M^{-1}·s^{-1} were obtained at 283, 298, and 313 K, respectively. According to the literature,[17] the maximum diffusion collision

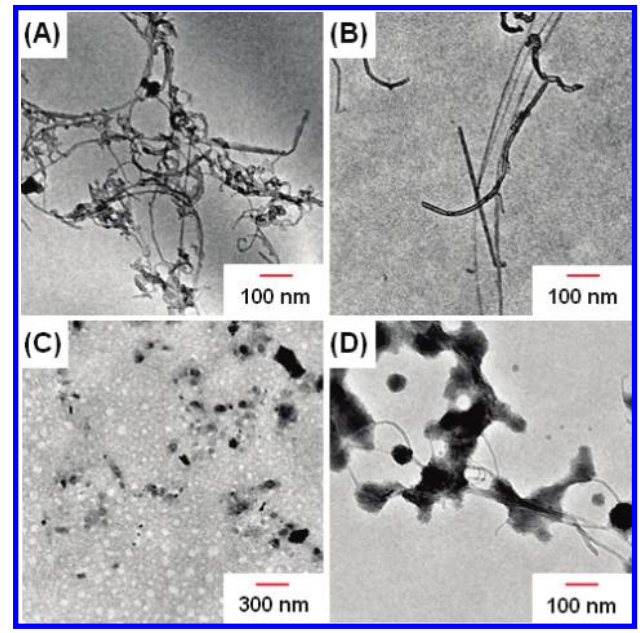

Figure 7. TEM images of nanotubes and their mixture with BSA: (A) raw multiwalled carbon nanotubes; (B) purified and carboxylated MWCNTs; (C) bovine serum albumin; (D) BSA−MWCNT conjugates.

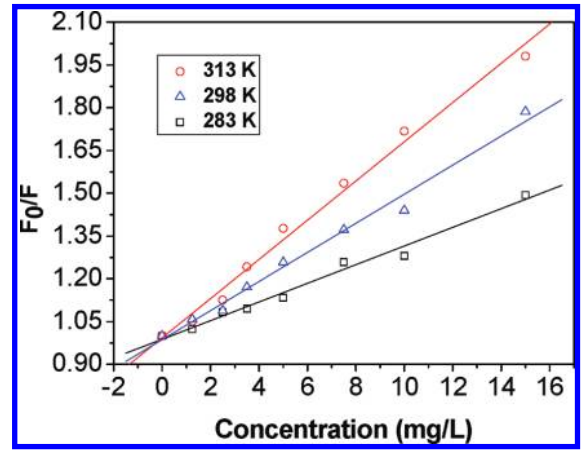

Figure 8. Stern−Volmer plots of fluorescence quenching for protein with MWCNTs at different temperatures. The result was obtained by taking the average of three replicate runs.

TABLE 2: Thermodynamic Parameters for Interaction of MWCNTs with BSA at 283, 298, and 313 K

T (K)	$K°$ (M^{-1})	$\Delta G°$ ($J \cdot mol^{-1}$)	$\Delta S°$ ($J \cdot mol^{-1} \cdot K^{-1}$)	$\Delta H°$ ($J \cdot mol^{-1}$)
283	$0.0763/\lambda^{0.958}$	$-10.4 \times 10^3 + 2.49 \times 10^3 \ln \lambda$		
298	$0.0492/\lambda$	$-9.67 \times 10^3 + 2.48 \times 10^3 \ln \lambda$	$41.0 - 0.828 \ln \lambda$	$7.30 \times 10^3 + 2.23 \times 10^3 \ln \lambda$
313	$0.0226/\lambda^{1.14}$	$-9.53 \times 10^3 + 2.67 \times 10^3 \ln \lambda$		

TABLE 3: Comparison of Binding Constant of MWCNTs to BSA before and after the Addition of the Molecular Probes

K (without the site probe) (M^{-1})	K (with Dig) (M^{-1})	K (with PB) (M^{-1})	K (with FA) (M^{-1})
$0.0492/\lambda$	$0.0992/\lambda^{0.667}$	$0.0602/\lambda^{0.523}$	$0.0324/\lambda^{1.17}$

rate constant of various quenchers with the biopolymer was 2.0×10^{10} $L \cdot mol^{-1} \cdot s^{-1}$. Hence, the higher value obtained here means that the quenching of Trp fluorescence occurred by a specific interaction between BSA and MWCNTs.[28] This analysis implies that the dominating quenching mechanism was static quenching and the increasing temperature was able to reduce the stability of the complex formation of the bioconjugates.[29]

Fluorescence lifetime measurement was introduced to distinguish between dynamic and static quenching. The time-resolved decay of BSA under different experimental conditions was taken at 280 nm. The data fit well to the sum of a single exponential decay with a χ^2 value close to 1.00. With the increasing concentration of MWCNTs, there is no obvious change in the decay profile of BSA. Since excited-state dynamic quenching is not expected to have a stable lifetime, the invariance of the lifetime for different amounts of MWCNTs should be attributed to another mechanism. An increasing amount of quencher did not significantly change the average lifetime, confirming the absence of a static quenching mechanism. This result also supports the adsorption of BSA on the surface of MWCNTs and the formation of a ground state surface complex.

3.3.2. Thermodynamic Analysis and the Nature of the Binding Forces. Results from fluorescence measurements can be used to estimate the binding constant of the BSA−MWCNT hybrid complex by a different form of the Stern−Volmer equation:[30]

$$\log \frac{F_0 - F}{F} = \log K_A + n \log[Q] \qquad (3)$$

where F_0, F, and [Q] are the same as in eq 2, n is the number of average binding sites, and K_A is the binding constant. Here,

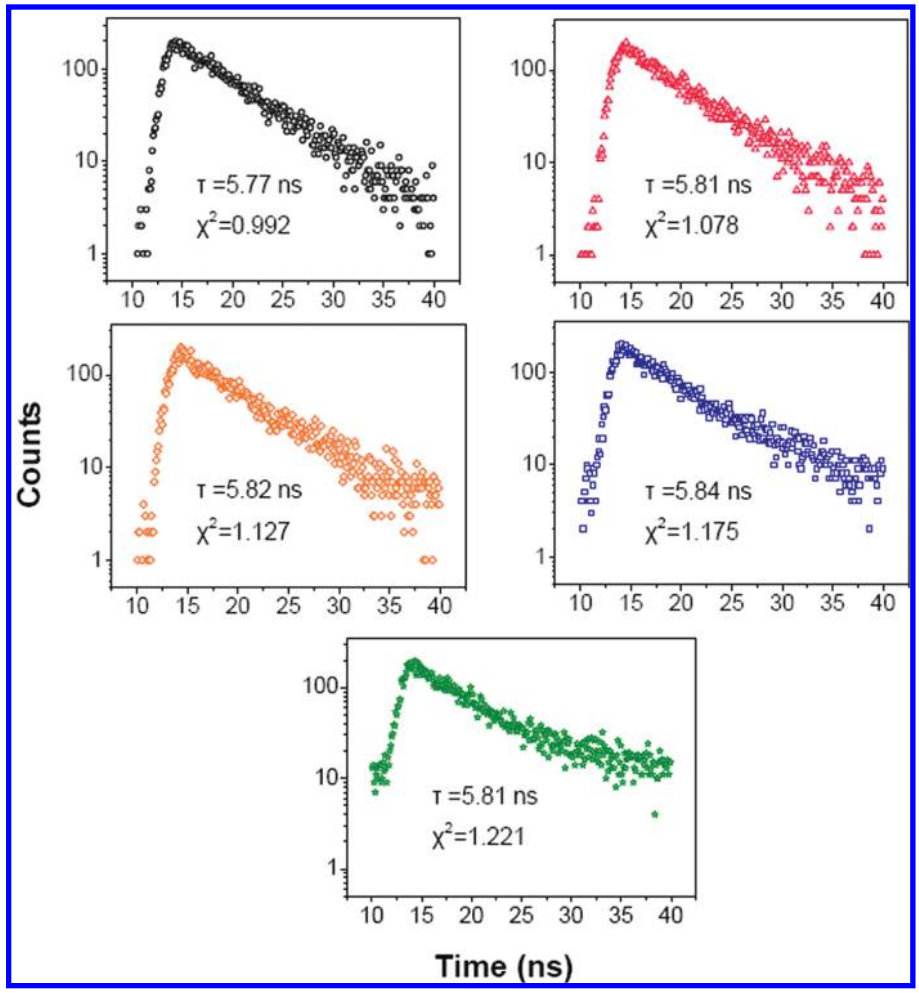

Figure 9. Time-resolved fluorescence decay profile of BSA monitored at the emission maximum for BSA with MWCNTs. Concentrations of MWCNTs from 1 to 5 were 0, 3, 6, 10, and 15 mg/L.

we substitute weight concentration multiplied by λ for molar concentration again.

A plot of $\log[(F_0 - F)/F]$ vs log[MWCNTs] yields $\log K_A$ as the intercept on the y axis and n as the slope (see SI Figure 4, Supporting Information). The binding constants obtained at 313, 298, and 283 K are given in Table 2.

Generally speaking, the interaction forces between nanoparticles and proteins include hydrogen bonds, van der Waals forces, electrostatic forces, and hydrophobic interaction forces. According to Ross' report,[31] the main binding forces can be judged by thermodynamic parameters. From the viewpoint of thermodynamics, $\Delta H^\circ > 0$ and $\Delta S^\circ > 0$ imply a hydrophobic interaction is the main force; $\Delta H^\circ < 0$ and $\Delta S^\circ < 0$ reflect van der Waals forces or hydrogen bonding; $\Delta H^\circ < 0$ and $\Delta S^\circ > 0$ suggest electrostatic forces play a key role. When there is no significant change in temperature, the enthalpy of the reaction can be considered as a constant in the formulas by which we calculated the thermodynamic parameters:

$$\ln\left(\frac{K_2}{K_1}\right) = \frac{\Delta H^\circ}{R}\left(\frac{1}{T_1} - \frac{1}{T_2}\right) \quad (4)$$

$$\Delta G^\circ = \Delta H^\circ - T\Delta S^\circ = -RT \ln K^\circ \quad (5)$$

where ΔH°, ΔG°, and ΔS° are enthalpy change, free enthalpy change, and entropy change, respectively. R is the gas constant 8.314 $J \cdot mol^{-1} \cdot K^{-1}$, and T is the temperature. K° represents the binding constant at the corresponding temperature. Results were shown in Table 2. The positive value of ΔS° and the negative value of ΔH° reveal the predominance of electrostatic interactions in the binding of MWCNTs with BSA.

3.3.3. Investigation into the Locations of the Main Binding Sites. In quest of the exact binding sites of BSA to MWCNTs, molecular probes which have special tight binding sites were used for displacement studies using fluorescence as a measurement tool. The pattern of displacement of MWCNTs by the probes enabled the identification of three binding sites on BSA. In connection with Sudlow's classification, digitoxin, phenylbutazone, and flufenamic acid show affinity for domains I, II, and III (SI Figure 5, Supporting Information), respectively.[32] Table 3 shows the fluorescence changes of MWCNTs bound to BSA. MWCNTs were significantly displaced by all three drugs, suggesting a nonspecific binding mode to BSA.

4. Conclusions

In summary, BSA noncovalently attached to MWCNTs at the expense of partly losing its secondary and tertiary structure. By means of spectroscopic techniques, we discovered that BSA could nonspecifically bind to MWCNTs through electrostatic interaction. The analysis of fluorescence lifetime showed that the fluorescence intensity of the protein was quenched by MWCNTs following a static mechanism. Distinct modes of the interaction were found on the basis of Scatchard calculations. From the electronic transitions observed by UV−vis spectrophotometry, we have discovered and interpreted the microenvironment changes of the backbone chains induced by different amounts of MWCNTs. This work not only provides the mechanism of BSA absorbed onto MWCNTs but also creates an approach for evaluation of protein conformations. Studies are ongoing in our laboratory to reveal the mechanism of size-dependent and functional-group-density-dependent impact of nanoparticles targeted to proteins. The same method may be used to study the biological behavior of other biomacromolecules in nanoparticle introduced systems.

Acknowledgment. This work is supported by NSFC (20875055), the Cultivation Fund of the Key Scientific and Technical Innovation Project, Ministry of Education of China (708058), NCET-06-0582, and Foundation for Middle Young Scientists and Key Science-Technology Project in Shandong Province (2007BS08005, 2008GG10006012). The authors gratefully thank Dr. Pamela Holt for editing the manuscript.

Supporting Information Available: Working curve of MWCNT solution, TGA results, ionic strength data Stern−Volmer plot, and illustration for three domains of BSA. This material is available free of charge via the Internet at http://pubs.acs.org.

References and Notes

(1) Iijima, S. *Nature* **1991**, *354*, 56.
(2) Magrez, A.; Kasas, S.; Salicio, V.; Pasquier, N.; Seo, J. W.; Celio, M.; Catsicas, S.; Schwaller, B.; Forro, L. *Nano Lett.* **2006**, *6*, 1121.
(3) Service, R. F. *Science* **2003**, *300*, 243.
(4) Brumfiel, G. *Nature* **2003**, *424*, 246.
(5) Lam, C. W.; James, J. T.; McCluskey, R.; Hunter, R. L. *Toxicol. Sci.* **2004**, *77*, 126.
(6) Wang, H. F.; Wang, J.; Deng, X. Y.; Sun, H. F.; Shi, Z. J.; Gu, Z. N.; Liu, Y. F.; Zhao, Y. L. *J. Nanosci. Nanotechnol.* **2004**, *4*, 1019.
(7) Azamian, B. R.; Davis, J. J.; Coleman, K. S.; Bagshaw, C. B.; Green, M. L. H. *J. Am. Chem. Soc.* **2002**, *124*, 12664.
(8) Matsuura, K.; Saito, T.; Okazaki, T.; Ohshima, S.; Yumura, M.; Iijima, S. *Chem. Phys. Lett.* **2006**, *429*, 497.
(9) Huang, W. J.; Taylor, S.; Fu, K. F.; Lin, Y.; Zhang, D. H.; Hanks, T. W.; Rao, A. M.; Sun, Y. P. *Nano Lett.* **2002**, *2*, 311.
(10) Mu, Q. X.; Liu, W.; Xing, Y. H.; Zhou, H. Y.; Li, Z. W.; Zhang, Y.; Ji, L. H.; Wang, F.; Si, Z. K.; Zhang, B.; Yan, B. *J. Phys. Chem. C* **2008**, *112*, 3300.
(11) Elgrabli, D.; Abella-Gallart, S.; Aguerre-Chariol, O.; Robidel, F.; Rogerieux, F.; Boczkowski, J.; Lacroix, G. *Nanotoxicology* **2007**, *1*, 266.
(12) Nepal, D.; Geckeler, K. E. *Small* **2007**, *3*, 1259.
(13) Edri, E.; Regev, O. *Anal. Chem.* **2008**, *80*, 4049.
(14) Matayoshi, E. D.; Wang, G. T.; Krafft, G. A.; Erickson, J. *Science* **1990**, *247*, 954.
(15) Gu, Q.; Kenny, J. E. *Anal. Chem.* **2009**, *81*, 420.
(16) Gentili, P. L.; Ortica, F.; Favaro, G. *J. Phys. Chem. B* **2008**, *112*, 16793.
(17) Zhao, L. Z.; Liu, R. T.; Zhao, X. C.; Yang, B. J.; Gao, C. Z.; Hao, X. P.; Wu, Y. Z. *Sci. Total Environ.* **2009**, *407*, 5019.
(18) Zhong, J.; Song, L.; Meng, J.; Gao, B.; Chu, W. S.; Xu, H. Y.; Luo, Y.; Guo, J. H.; Marcelli, A.; Xie, S. S.; Wu, Z. Y. *Carbon* **2009**, *47*, 967.
(19) Li, Z. Y.; Abramavicius, D.; Zhuang, W.; Mukamel, S. *Chem. Phys.* **2007**, *341*, 29.
(20) Liu, R. T.; Sun, F.; Zhang, L. J.; Zong, W. S.; Zhao, X. C.; Wang, L.; Wu, R. L.; Hao, X. P. *Sci. Total Environ.* **2009**, *407*, 4184.
(21) McConnell, H. *J. Chem. Phys.* **1952**, *20*, 700.
(22) Bayliss, N. S.; McRae, E. G. *J. Phys. Chem.* **1954**, *58*, 1002.
(23) Ungnade, H. E. *J. Am. Chem. Soc.* **1953**, *75*, 432.
(24) Brooker, L. G. S.; Keyes, G. H.; Sprague, R. H.; VanDyke, R. H.; VanLare, E.; VanZandt, G.; White, F. L.; Cressman, H. W. J.; Dent, S. G., Jr. *J. Am. Chem. Soc.* **1951**, *73*, 5332.
(25) Cheng, X. X.; Lui, Y.; Zhou, B.; Xiao, X. H.; Liu, Y. *Spectrochim. Acta, Part A* **2009**, *72*, 922.
(26) He, P. L.; Hu, N. F. *J. Phys. Chem. B* **2004**, *108*, 13144.
(27) Lakowicz, J. R.; Weber, G. *Biochemistry* **1973**, *12*, 4161.
(28) Ware, W. R. *J. Phys. Chem.* **1962**, *66*, 455.
(29) Shang, L.; Wang, Y. Z.; Jiang, J. G.; Dong, S. J. *Langmuir* **2007**, *23*, 2714.
(30) Charbonneau, D.; Beauregard, M.; Tajmir-Riahi, H. A. *J. Phys. Chem. B* **2009**, *113*, 1777.
(31) Ross, P. D.; Subramanian, S. *Biochemistry* **1981**, *20*, 3096.
(32) Sudlow, G.; Birkett, D. J.; Wade, D. N. *Mol. Pharmacol.* **1976**, *12*, 1052.

JP100903X